8298 *Inorg. Chem.* **2010**, *49*, 8298–8304
DOI: 10.1021/ic1006617

Inorganic Chemistry
Article

Oxygen Close-Packed Structure in Amorphous Indium Zinc Oxide Thin Films

Tatsuya Eguchi,[†] Hiroyuki Inoue,*[,†] Atsunobu Masuno,[†] Koji Kita,[‡] and Futoshi Utsuno[§]

[†]*Institute of Industrial Science, the University of Tokyo, 4-6-1 Komaba, Meguro-ku, Tokyo, 153-8505 Japan,* [‡]*Department of Materials Engineering, the University of Tokyo, 7-3-1 Hongo, Bunkyo-ku, Tokyo, 113-0033 Japan, and* [§]*Idemitsu Kosan, Co., Ltd., 1280 Kamiizumi, Sodegaura-shi, Chiba, 299-0293 Japan*

Received April 7, 2010

Amorphous indium zinc oxide (IZO) thin film structures of varying amounts of Zn content were investigated using X-ray diffraction measurements and molecular dynamics (MD) simulations. The characteristic amorphous structure having high oxygen coordination number and edge-shared polyhedra were confirmed using both techniques. Detailed analysis of the structural model revealed that the oxygen close-packed structure was almost realized in the nanometer range. It was also found that the number of Zn ions occupying the tetrahedral site of the oxygen close-packed structure increased with increasing ZnO content although In ions occupied the octahedral site. We conclude that the amorphous structure stability of the indium zinc oxide thin films is enhanced by the existence of Zn ions in the tetrahedral site, which block In ions in the octahedral site ordering similar to that in an In_2O_3 crystal.

1. Introduction

Transparent conductive oxide (TCO) thin films are widely used as electrodes in various applications such as liquid crystal displays, plasma displays, solar cells, and organic light emitting diodes.[1−5] Among many TCOs, amorphous indium zinc oxide (a-IZO) thin films have received much attention because of their very smooth surface, availability of plastic substrate, and good chemical etchability.[6−12] Electrical properties of a-IZO thin films have been reported as functions of their composition and their preparation conditions.[13−20] For example, the carrier density and Hall mobility were varied from 6×10^{20} to 2.65×10^{16} cm^{-3} and from 10 to 51 $cm^2/(V\ s)$, respectively, by varying the deposition parameters such as O_2 or H_2 flow ratios.[21] It has also been reported that amorphous phase stability was enhanced with increasing ZnO content.[22] In order to understand and control physical properties and structural stability, additional information about the atomic arrangement of the a-IZO thin films is required. The grazing incident X-ray scattering (GIXS) technique is well suited for structural analysis of thin films because it can obtain structural information of a thin film without any contribution from the substrate. Utsuno and co-workers obtained the radial distribution functions (RDFs) of amorphous In_2O_3 and a-IZO thin films using the GIXS technique.[23,24] Using RDFs,

*To whom correspondence should be addressed. E-mail: inoue@iis.u-tokyo.ac.jp; tel.: +81-3-5452-6315; fax: +81-3-5452-6316.

(1) Kamiya, T.; Hosono, H. *NPG Asia Mater*. **2010**, *2*, 15–22.
(2) Minami, T. *Semicond. Sci. Technol.* **2005**, *20*, S35–S44.
(3) Ginley, D. S.; Bright, C. *MRS Bull*. **2000**, *25*, 15–21.
(4) Lewis, B. G.; Paine, D. C. *MRS Bull*. **2000**, *25*, 22–27.
(5) Gordon, R. G. *MRS Bull*. **2000**, *25*, 52–57.
(6) Sasabayashi, T.; Ito, N.; Nishimura, E.; Kon, M.; Song, P. K.; Utsumi, K.; Kaijo, A.; Shigesato, Y. *Thin Solids Films* **2003**, *445*, 219–223.
(7) Sato, Y.; Taketomo, M.; Ito, N.; Miyamura, A.; Shigesato, Y. *Thin Solid Films* **2008**, *516*, 4598–4602.
(8) Cho, S.-W.; Jeong, J.-A; Bae, J.-H.; Moon, J.-M.; Choi, K.-H.; Jeong, S. W.; Park, N.-J.; Kim, J.-J.; Lee, S. H.; Kang, J.-W.; Yi, M.-S.; Kim, H.-K. *Thin Solid Films* **2008**, *516*, 7881–7885.
(9) Zeng, K.; Zhu, F.; Hu, J.; Shen, L.; Zhan, K.; Gong, H. *Thin Solid Films* **2003**, *443*, 60–65.
(10) Paine, D. C.; Yaglioglu, B.; Beiley, Z.; Lee, S. *Thin Solid Films* **2008**, *516*, 5894–5898.
(11) Fortunato, E.; Barquinha, P.; Pimentel, A.; Pereira, L.; Gonçalves, G.; Martins, R. *Phys. Stat. Sol.* (*RRL*) **2007**, *1*, R34–R36.
(12) Wang, Y.-L.; Ren, F.; Lim, W.; Norton, D. P.; Pearton, S. J.; Kravchenko, I. I.; Zavada, J. M. *Appl. Phys. Lett*. **2007**, *90*, 232103.
(13) Moriga, T.; Okamoto, T.; Hiruta, K.; Fujiwara, A.; Nakabayashi, I.; Tominaga, K. *J. Solid State Chem*. **2000**, *155*, 312–319.
(14) Nishiura, E.; Sasabayashi, T.; Ito, N.; Sato, Y.; Utsumi, K.; Yano, K.; Kaijo, A.; Inoue, K.; Shigesato, Y. *Jpn. J. Appl. Phys*. **2007**, *46*, 7806–7811.
(15) Ku, D. Y.; Kim, I. H.; Lee, I.; Lee, K. S.; Lee, T. S.; Jeong, J.-h.; Cheong, B.; Baik, Y.-J.; Kim, W. M. *Thin Solid Films* **2006**, *515*, 1364–1369.
(16) Leenheer, A. J.; Perkins, J. D.; van Hest, M. F. A. M.; Berry, J. J.; O'Hayre, R. P.; Ginley, D. S. *Phys. Rev. B* **2008**, *77*, 115215.
(17) Martins, R.; Almeida, P.; Barquinha, P.; Pereira, L.; Pimentel, A.; Ferreira, I.; Fortunato, E. *J. Non-Cryst. Solids* **2006**, *352*, 1471–1474.
(18) Ito, N.; Sato, Y.; Song, P. K.; Kaijio, A.; Inoue, K.; Shigesato, Y. *Thin Solid Films* **2006**, *496*, 99–103.
(19) Jung, Y. S.; Seo, J. Y.; Lee, D. W.; Jeon, D. Y. *Thin Solid Films* **2003**, *445*, 63–71.
(20) Mikawa, M.; Moriga, T.; Sakakibara, Y.; Nisaki, Y.; Murai, K.; Nakabayashi, I.; Tominaga, K. *Mater. Res. Bull*. **2005**, *40*, 1052–1058.
(21) Ashida, T.; Miyamura, A.; Sato, Y.; Yagi, T.; Taketoshi, N.; Baba, T.; Shigesato, Y. *J. Vac. Sci. Technol. A* **2007**, *25*, 1178–1183.
(22) Taylor, M. P.; Readey, D. W.; van Hest, M. F. A. M.; Teplin, C. W.; Alleman, J. L.; Dabney, M. S.; Gedvilas, L. M.; Keyes, B. M.; To, B.; Perkins, J. D.; Ginley, D. S. *Adv. Funct. Mater*. **2008**, *18*, 3169–3178.
(23) Utsuno, F.; Inoue, H.; Yasui, I.; Shimane, Y.; Tomai, S.; Matsuzaki, S.; Inoue, K.; Hirosawa, I.; Sato, M.; Honma, T. *Thin Solid Films* **2006**, *496*, 95–98.
(24) Utsuno, F.; Inoue, H.; Shimane, Y.; Shibuya, T.; Yano, K.; Inoue, K.; Hirosawa, I.; Sato, M.; Honma, T. *Thin Solid Films* **2008**, *516*, 5818–5821.

 Published on Web 08/24/2010

they estimated that the average coordination numbers around In and Zn ions in those films were 6 and 4, respectively. They also found that there were not only corner-shared InO_6 octahedra but also edge-shared ones. On the basis of their results, they suggested that the atomic arrangement around In ions in the amorphous In_2O_3 and a-IZO thin films resembled that in the bixbyite In_2O_3 crystal. However, the effect of an increase of ZnO content on the amorphous structure stability remains unclear. The characteristic structure observed in those films, which have high oxygen coordination number and edge-shared polyhedra, is rarely evident in conventional amorphous oxides, and therefore it is important to figure out the remaining problems of a-IZO thin films. It is now necessary to derive additional information beyond the coordination number or linkage patterns of polyhedra from the characteristic structure of a-IZO thin films.

In this study, we investigated the structure of a-IZO thin films using a combination of X-ray diffraction (XRD) measurements and molecular dynamics (MD) simulations. The characteristic amorphous structure constituted by oxygen octahedra was confirmed both experimentally and by calculation, and the structural properties clearly showed dependency on the ZnO content in a-IZO thin films. The first sharp diffraction peak (FSDP) in the interference functions demonstrated the existence of a local layer-like structure in the films. Detailed analysis on the structural model indicated the presence of a nearly close-packed structure of oxygen ions. It is suggested that the close-packed structure is responsible for the amorphous structure stability in a-IZO thin films.

2. Experimental Procedures

2.1. Sample Preparation and X-ray Diffraction Measurement. Amorphous indium zinc oxide thin films of more than 500 nm thickness were prepared using the r.f. sputtering method at 1.0 Pa in pure Ar gas. The targets used were three different indium−zinc compositions: $5In_2O_3 \cdot 2ZnO$, $7In_2O_3 \cdot 6ZnO$, and $In_2O_3 \cdot 2ZnO$. The substrate was silica glass of dimensions $20 \times 20 \times 1$ mm^3, located beside the target without heating. It was confirmed using X-ray diffraction that there were no crystalline phases in the thin films. Compositions of the thin films were determined by energy dispersive X-ray (EDX) spectroscopy and the thicknesses of the thin films were measured using a surface profiler (DEKTAK^3, Sloan Tech.). The densities of the thin films, about 30 nm thick, were estimated by grazing incidence angle X-ray reflectivity (GIXR) measurements in the 2θ range from 0.4 to 5°.[25]

Diffraction experiments were carried out using a Rigaku RINT2500 V with Mo Kα radiation. The incident angle δ was fixed at 1.0° and 2θ scans were taken from 3 to 146°. The diffraction intensity from a-IZO thin films I_{film} was given by

$$I_{film} = I_{obs} - I_{sub} \exp\left\{-\mu_f t_f \left(\frac{1}{\sin\delta} + \frac{1}{\sin 2\theta}\right)\right\} \quad (1)$$

where I_{obs} and I_{sub} are diffraction intensities of the sample and the substrate, respectively, μ_f is the absorption coefficient of the thin film, and t_f is the thickness of the thin film. The contribution from the substrate can be removed according to eq 1. After correcting the influence of the film thickness and polarization, a Krough−Moe−Norman normalization method was used to obtain coherent X-ray scattering intensity, $i(Q)$. Total correlation function, $T(r) = 4\pi r\rho(r)$, was obtained from the experimental amplitude function $Qi(Q)$ using Lorch function.[26]

Table 1. Interatomic Potential Parameters Used in MD Simulations[a]

ion		Z_i
In		1.95
Zn		1.5
O		−1.30 ∼ −1.3744
pair	B (J)	ρ (Å)
In−O	1.02×10^{-15}	0.23
Zn−O	6.06×10^{-16}	0.23
O−O	8.63×10^{-17}	0.36

[a] Z_i is effective charge, B is empirical constant, and ρ is softness parameter.

2.2. Molecular Dynamics Simulations. Born−Mayer interatomic potential functions used are given by

$$\Phi_{ij}(r_{ij}) = \frac{e^2}{4\pi\varepsilon_0}\frac{Z_i Z_j}{r_{ij}} + B_{ij}\exp\left(-\frac{r_{ij}}{\rho_{ij}}\right) \quad (2)$$

where Z_i is the effective charge of the ith ion, r_{ij} is the interatomic distance, B_{ij} is the empirical constant, and ρ_{ij} is the softness parameter. The effective charges of In and Zn ions were fixed and the charge of oxide ions was set to fill the charge neutrality. These initial parameters were given from the MD simulations for bixbyite In_2O_3 and wurtzite ZnO crystals.[27,28] Configurations containing 640 particles for In_2O_3 and 360 particles for ZnO were initially located at ideal atomic coordinates and then were evolved over 20 000 time steps at 293 K, using a time step of 1 fs. Some parameters sets maintained the crystal structure of bixbyite or wurtzite. From them, an optimal parameter set was determined so that the vibration frequencies obtained by Raman and infrared (IR) spectra could be produced. The final parameters are listed in Table 1. The effective charges of In and O ions in an In_2O_3 crystal were +1.95 and −1.3, respectively, and those of Zn and O ions in ZnO crystal were +1.5 and −1.5, respectively. Interatomic potential functions obtained for In−O and Zn−O reached a minimum at 1.79 and 1.71 Å, respectively. The calculated highest frequencies of Raman and IR active modes of bixbyite In_2O_3 using these parameters were 629 and 584 cm^{-1}, and the calculated frequencies of A_1 TO, E_1 TO, and two E_2 modes of ZnO wurtzite structure were 376, 418, 432, 115 cm^{-1}, respectively. These frequencies were in close agreement with previous experimental values of 637 and 602 cm^{-1},[29] and 380, 407, 437, and 101 cm^{-1},[30] respectively.

Structural models for a-IZO thin films were constructed using optimal parameters under the following conditions. The summations of the Coulombic interactions were evaluated using the Ewald summation method. Initial coordinates of the ions were given randomly in a cubic basic cell with periodic boundary conditions. The system was relaxed at 4000 K under a constant volume condition. The system was then quenched from 4000 to 293 K in 200 000 time steps, using a time step of 1 fs. After 20 000 time steps at 293 K, the atomic arrangement was evaluated from the coordinates. Five models for each composition were prepared from different initial coordinates. Structural models for the amorphous In_2O_3 thin films were also prepared for reference.

(25) Wiemer, C.; Ferrari, S.; Fanciulli, M.; Pavia, G.; Lutterotti, L. *Thin Solid Films* **2004**, *450*, 134–137.

(26) Wright, A. C.; *Experimental Techniques in Glass Science*; The American Ceramic Society: Westerville, OH, 1993.

(27) Marezio, M. *Acta Crystallogr.* **1966**, *20*, 723–728.

(28) Sawada, H.; Wang, R.; Sleight, A. W. *J. Solid State Chem.* **1996**, *122*, 148–150.

(29) White, W. B.; Keramidas, V. G. *Spectrochim. Acta A* **1972**, *28*, 501–509.

(30) Damen, T. C.; Porto, S. P. S.; Tell, B. *Phys. Rev.* **1966**, *142*, 570–574.

Table 2. Contents of ZnO, Densities and Thicknesses of In_2O_3 and a-IZO Thin Films

	ZnO (mol %)	density (g/cm^3)	thickness (nm)
Z00	0	7.1[a]	
Z24	24	7.0	500
Z44	44	6.8	1100
Z64	64	6.5	950

[a] Density is taken from bixbyite In_2O_3 crystals.

3. Results

3.1. Sample Characterization. The composition, thickness, and density of the films are listed in Table 2. According to EDX measurements, ZnO content of the films tended to decrease in comparison with the composition of the target. Here, a-IZO thin films are labeled Z24, Z44, and Z64 according to the ZnO mol %. The In_2O_3 film for simulation is labeled Z00.

3.2. X-ray Diffraction Measurements. Figure 1 shows the X-ray scattering intensities of Z24, Z44, and Z64, and the intensities separated into I_{film} and I_{sub} due to eq 1. The main peaks from silica substrate and a-IZO thin films were observed at 1.5 and 2.2 Å^{-1}, respectively. The peak heights of a-IZO thin films varied according to the film thickness. In Figure 2, X-ray interference functions $Qi(Q)$ that are obtained from the experiment are given. There were strong and sharp peaks at 2.2 Å^{-1} in $Qi(Q)$'s, and the heights decreased with an increase in the ZnO content. Figure 3 shows the total correlation functions $T(r)$ obtained from the Fourier transformation of the $Qi(Q)$'s. The heights of all peaks decreased with an increase in ZnO content. Three $T(r)$'s had almost the same shape, and the first peak was located between 2.12−2.14 Å; however, the curve of the Z24 film was a little sharper than the others. This value is close to the In−O distance in the In_2O_3 bixbyite crystal and the Zn−O distance in the ZnO wurtzite crystal. The In_2O_3 bixbyite crystal structure consists of InO_6 octahedra, in which the In−O distance is in the range 2.12−2.23 Å, with an average of 2.18 Å. ZnO wurtzite crystal consists of Zn−O tetrahedra and the Zn−O distance is in the range 1.97−1.99 Å. Therefore, the initial set of peaks of the $T(r)$'s could be indexed as In−O and Zn−O pairs. The second set of peaks, with a shoulder between 3.38−3.42 Å, could correspond to cation−cation pairs such as In−In, In−Zn, and Zn−Zn pairs. This was also confirmed by considering bond lengths in the In_2O_3 and ZnO crystals. In the In_2O_3 crystals, the InO_6 octahedron is surrounded by 12 octahedra. Six of the 12 octahedra share two oxygen ions with the central octahedron and the other six share one oxygen ion with it. Thus, two kinds of In−In pairs are formed with distances in the range 3.35−3.36 Å and 3.82−3.84 Å in In_2O_3 crystals. The shorter distances are between In ions in the edge-shared octahedra and the longer ones are between In ions in the corner-shared octahedra. In the ZnO crystal, the distances between Zn−Zn pairs are 3.21−3.25 Å, which is shorter than the In−In distance in the In_2O_3 crystal. That the second peaks in the $T(r)$'s shifted to the shorter distance side as the ZnO content increased is considered a result of increases in the contributions of Zn−Zn and Zn−In pairs. The third peak overlaps the peaks at 5.8 and 6.7 Å.

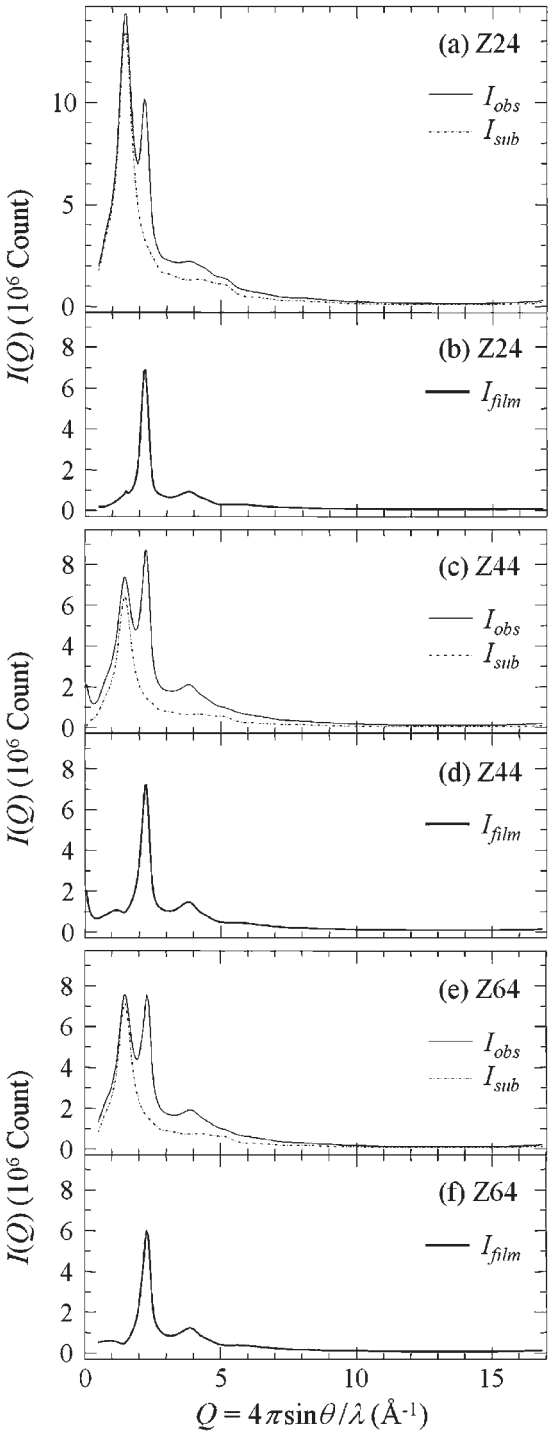

Figure 1. X-ray scattering intensities obtained from X-ray diffraction measurements for (a, b) Z24, (c, d) Z44, and (e, f) Z64. Thin solid lines are for measured intensities I_{obs}, dashed lines are for Si substrate I_{sub}, and bold solid lines are for thin films I_{film}.

3.3. Molecular Dynamics Simulations. The number of ions in basic cells and the cell sizes are listed in Table 3. Table 4 shows the oxygen coordination number distribution of In and Zn ions in the structural models for the In_2O_3 and the a-IZO thin films. The distributions of the In−O and Zn−O length have the first peaks at 2.11−2.13 and 2.02−2.03 Å, respectively, with FWHMs of 0.2 Å. The cutoff distance that determines the oxygen coordination number was 2.9 Å for both In−O and Zn−O pairs.

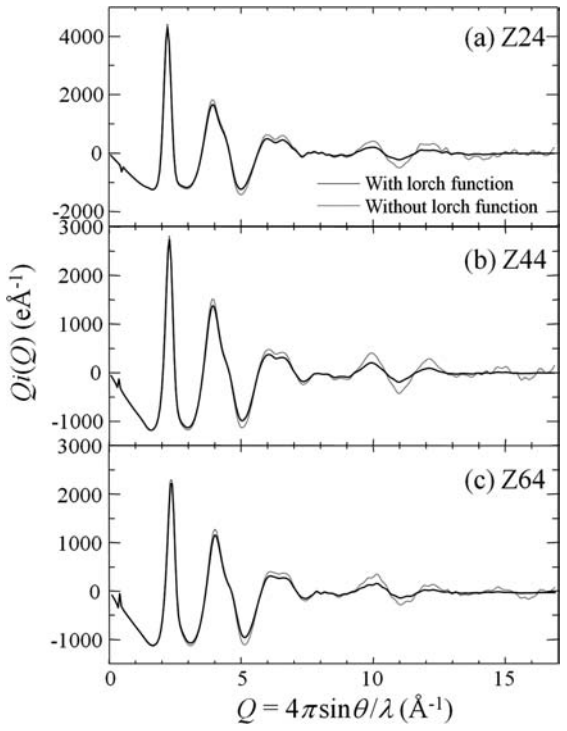

Figure 2. Interference function curves for (a) Z24, (b) Z44, and (c) Z64. Solid lines and dotted lines are obtained using lorch function and without lorch function, respectively.

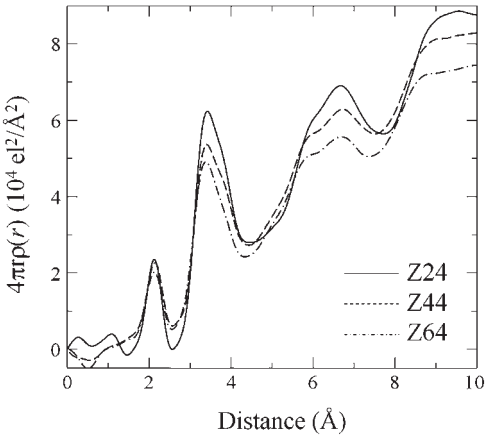

Figure 3. Total correlation functions $T(r)$ of Z24 (solid line), Z44 (dashed line), and Z64 (dashed-dotted line).

Table 3. Numbers of Ions and Cell Sizes in Basic Cells for In_2O_3 and a-IZO Thin Films

sample	In	Zn	O	cell size (Å^3)
Z00	1200		1800	33.8990
Z24	1044	156	1722	33.4379
Z44	864	336	1632	33.0079
Z64	636	564	1518	32.4844

The oxygen coordination numbers were found to vary widely from 4 to 7 and their distribution shifted to lower coordination numbers with an increase in ZnO content. The average oxygen coordination numbers of In and Zn ions were 5.8−5.6 and 5.3−5.0, respectively.

In Figure 4, the total correlation function $T(r)$ calculated by MD simulations are shown together with experimental results. Wright[31] proposed that the agreement between experimental and simulated total correlation

Table 4. Fraction of 4-, 5-, 6-, and 7-Fold Coordinated In and Zn Ions by Oxygen Ions, and Average Oxygen Coordination Number of In and Zn Ions in Structural Models for In_2O_3 and a-IZO Thin Films

		fraction of n-fold In and Zn (%)				
sample	coordinated ion	4	5	6	7	average oxygen coordination number
Z00	In	1	23	70	6	5.81
Z24	In	1	25	70	4	5.77
	Zn	12	50	36	2	5.28
Z44	In	1	31	65	3	5.70
	Zn	17	52	31	0	5.14
Z64	In	2	37	60	1	5.60
	Zn	24	52	24	0	5.00

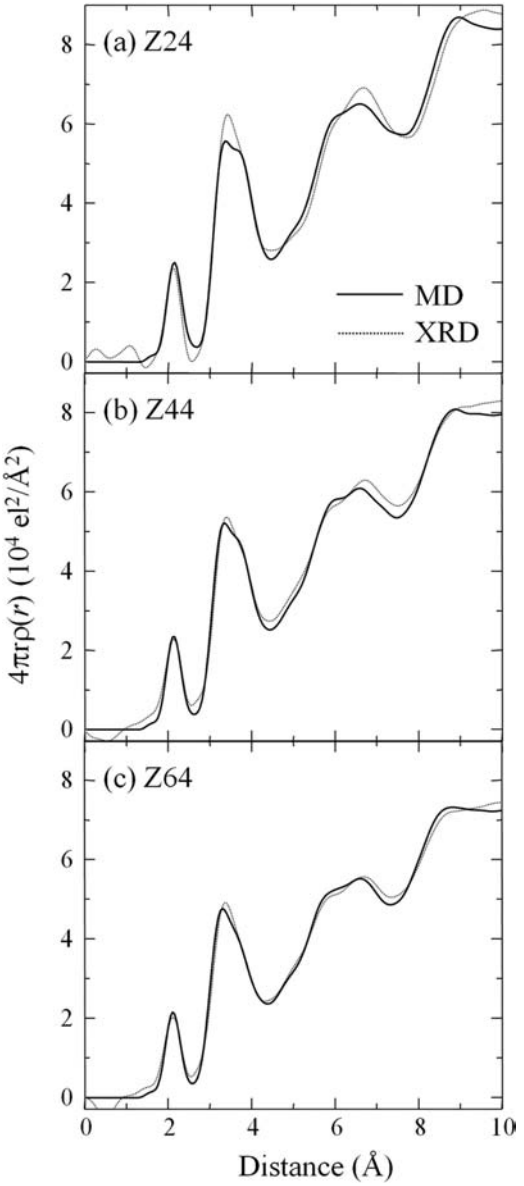

Figure 4. Total correlation functions $T(r)$ of (a) Z24, (b) Z44, and (c) Z64. Solid lines are from MD simulations and dotted lines are from experimental results.

(31) Wright, A. C. *J. Non-Cryst. Solids* **1993**, *159*, 264–268.

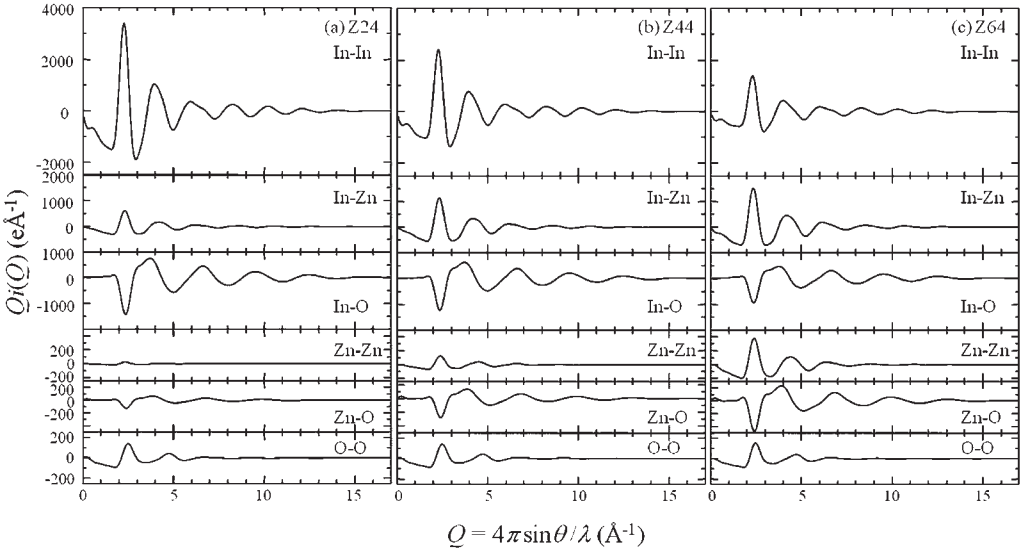

Figure 5. Partial interference function curves for (a) Z24, (b) Z44, and (c) Z64.

functions is quantified by the calculation of an $R\chi$ factor, defined as follows:

$$R\chi = \left[\frac{\sum_i \left(T_{\mathrm{exp}}(r_i) - T_{\mathrm{sim}}(r_i)\right)^2}{\sum_i \left(T_{\mathrm{exp}}(r_i)\right)^2}\right]^{1/2} \quad (3)$$

The $R\chi$ factors calculated over the range 0−10 Å were 5.5, 4.1, and 3.9% for Z24, Z44, and Z64, respectively. These small $R\chi$ values indicate close agreement between experimental $T(r)$'s and calculated values. The observed and calculated total correlation functions increasingly improved as the content of ZnO increased. However, apparent discrepancies at 3.4 and 6.7 Å were seen in the $T(r)$ of Z24. Partial correlation functions can be used to find the origin of discrepancies. Figure 5 shows the calculated partial interference functions for Z24, Z44, and Z64. It is clearly seen that the In−In pair had the biggest contribution in the total correlation function at 3.4 and 6.7 Å. This indicated that the apparent discrepancies in Z24 were caused by a slightly higher order arrangement of In ions in real films than that of MD simulations.

The proportions of linkage patterns between a central polyhedron and coordinating polyhedra are listed in Table 5. An In or Zn polyhedron was found to be surrounded by 11 or 12 polyhedra, as seen in the column of total coordination number. It shared its corners with 7 or 8 polyhedra and its edges with four polyhedra, which are the total numbers of InO_n and ZnO_n polyhedra. It is clearly seen that the numbers of InO_n polyhedra surrounding an In or Zn ion decreased with increasing ZnO content for corner-, edge-, and face-sharing linkages, while those of ZnO_n polyhedra increased, depending on the chemical composition. The proportion of the edge- and corner-sharing linkages, however, was hardly changed by the composition. For example, the total number of InO_n and ZnO_n corner-sharing with In ions of Z24, Z44, and Z64 are 7.7, 7.8, and 7.8, respectively. Those edge-sharing with Zn ions of Z24, Z44, and Z64 are 3.8, 3.9, and 3.8, respectively.

Table 5. Numbers of InO_n and ZnO_n Polyhedra Coordinating an In or Zn Ion in Structural Models for In_2O_3 and a-IZO Thin Films[a]

		InO_n			ZnO_n			
sample	central ion	corner	edge	face	corner	edge	face	total
Z00	In	7.3	4.2	0.4				11.9
Z24	In	6.7	3.6	0.3	1.0	0.5	0.1	12.2
	Zn	6.4	3.4	0.3	0.9	0.4	0.0	11.4
Z44	In	5.7	3.1	0.3	2.1	1.1	0.1	12.4
	Zn	5.3	2.9	0.3	2.0	1.0	0.1	11.6
Z64	In	4.2	2.4	0.2	3.6	2.0	0.1	12.5
	Zn	4.1	2.2	0.2	3.5	1.6	0.1	11.7

[a] Linkage patterns between central polyhedron and neighborhood polyhedra are corner-, edge-, and face-sharing.

The proportions of the number of In and Zn ions around an oxygen ion are listed in Table 6. Seventy-six percent of oxygen ions are surrounded by four In ions in Z00. In Z24, the proportion of 4-fold oxygen ions decreased, while that of 3-fold or lower-fold oxygen ions increased. The number of Zn ions coordinating an oxygen ion is zero or one because of the low concentration of ZnO in Z24. With increasing ZnO content, the numbers of In ions coordinating an oxygen ion decrease. In contrast, those of Zn ions increased and they are distributed at the center of 3-fold oxygen ions. It is noted that in all cases the average coordination number of In + Zn is about 4, although the coordination number slightly increased with an increase in ZnO content. This means that one oxygen ion is surrounded by four cations and the value was hardly changed by the composition, although the ratios of In, Zn, and In + Zn did change by the compositions.

4. Discussion

In the structural models for the a-IZO thin films, we accurately found the composition dependence of coordination numbers and their distributions. Considering that the framework of the a-IZO structure is constructed by the In−O and Zn−O bonds, the a-IZO structures obtained both experimentally and through simulation are obviously incompatible with the well-known Zachariasen's rules of glass formation. For example, the average coordination numbers

Table 6. Fraction of Numbers of In, Zn, and In + Zn Ions Coordinating an Oxygen Ion in the Structural Models of In_2O_3 and a-IZO Thin Films[a]

		fraction of *n*-fold O(%)							average coordination number
sample		0	1	2	3	4	5	6	
Z00	In	0	0	0	18	76	6	0	3.9
Z24	In	0	1	7	38	50	4	0	3.5
	Zn	60	33	6	1	0			0.5
	In + Zn				13	77	10	0	4.0
Z44	In	0	4	22	43	29	2	0	3.0
	Zn	31	40	22	6	1	0		1.1
	In + Zn				10	74	16	0	4.1
Z64	In	3	16	37	32	11	1		2.4
	Zn	10	29	35	19	6	1		1.9
	In + Zn				6	69	23	2	4.2

[a] Average coordination number of cations surrounding an oxygen ion are also shown.

of In and Zn ions were 5.8 to 5.0, while that of conventional glass is about 3 or 4. There were not only corner-sharing linkages between the coordinated polyhedra but also edge-sharing ones. The cation coordination number around the oxygen ions was about 4, which is too high for conventional glasses. Even though Zachariasen's rules are inapplicable in a-IZO thin films these films are still stable. Therefore, we need to reconsider the structure of a-IZO thin films beyond the coordination numbers and the linkage patterns of polyhedra.

The first sharp diffraction peak (FSDP) on the interference function $Qi(Q)$ gives us one of the solutions for this question. In Figure 2, there were relatively large peaks on the interference functions for Z24, Z44, and Z64 films located at 2.22, 2.28, and 2.34 $Å^{-1}$, respectively. These values are converted to d values of 2.83, 2.76, and 2.69 Å, respectively, using $d = 2\pi/Q$. However, there are no definite peaks on the total correlation function at 2.83, 2.76, and 2.69 Å, respectively. Therefore, FSDPs show the existence of a plane that separates the intervals. The partial interference functions for each pair, which is obtained from each calculated partial correlation function, are shown in Figure 5. It is clearly seen that there are positive or negative peaks at about 2.3 $Å^{-1}$ in all partial interference functions for Z24, Z44, and Z64. The peak positions in Z24, for example, were varied from 2.28 $Å^{-1}$ on In−In pairs to 2.52 $Å^{-1}$ on O−O pairs, which also indicated the existence of the layer structure of intervals from 2.76 to 2.49 Å.

The distribution of O−O pairs gives us another solution for our question. Figure 6 shows the distribution of O−O pairs and oxygen coordination number around an oxygen ion in the structural models for Z64. The distribution and coordination number were almost the same as those of other a-IZO thin films. It is clearly seen from the distribution curve that the nearest neighboring oxygen ions around an oxygen ion are located within a broad distribution of 2.5−3.9 Å. The coordination number accumulated in the range up to 3.9 Å is about 12. A previous report about our MD simulations revealed that a drastic structural change occurred when the radius of the cation increases over a certain value.[32] When the radius of the cation is small, the atomic arrangement consists of the coordinated polyhedron and their corner-sharing linkage. In that case, the coordination number of the cation shows

(32) Inoue, H.; Utsuno, F.; Yasui, I. *J. Non-Cryst. Solids* **2004**, *349*, 16–21.

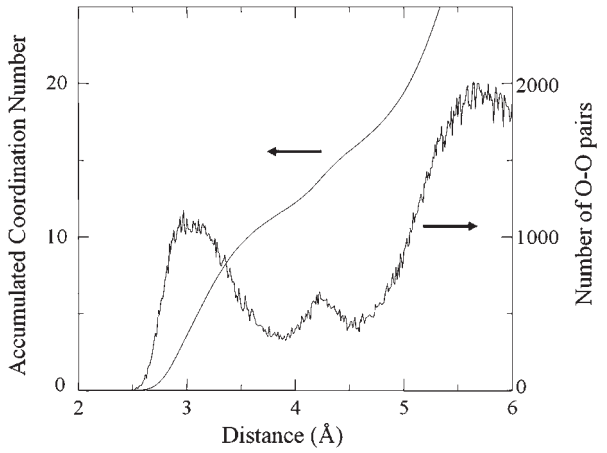

Figure 6. Distribution of O−O pairs. Accumulated oxygen coordination number (left side) and number of O−O pairs (right side).

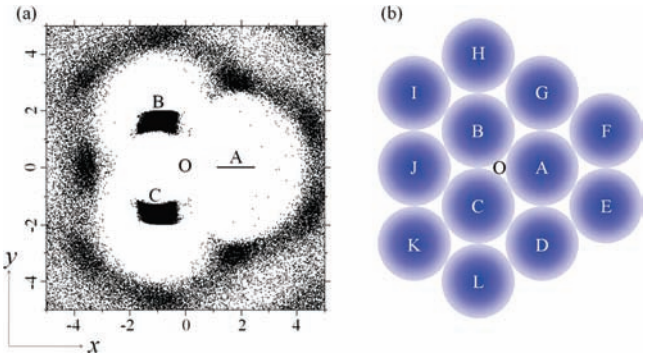

Figure 7. (a) Reduced atomic arrangement of Z64 with the xy range of 10 × 10 Å and ±0.5 Å in the z direction. Dots represent oxygen ions and the origin is O. A, B, and C are places of the three selected oxygen ions. (b) Illustration of oxygen close-packed structure appearing in reduced atomic arrangement. Each sphere corresponds to the place of high concentration of dots in (a) and was labeled as from A to L.

a constant value for any value of cation radius. However, when the radius of the cation increases over a certain value, the structure composed of the polyhedra is collapsed and a quasi close-packed structure of the oxygen ions is formed. The large value of 12 for the oxygen coordination number in the structural models for a-IZO thin films indicates that the atomic arrangement may be similar to that of the close-packed structure of oxygen ions.

The oxygen close-packed structure can be seen in the reduced atomic arrangement described below. In the structural model produced by MD simulation, any three neighboring oxygen ions are selected and put on an xy plane. The origin of the plane is the center of gravity of the three oxygen ions. One of the three oxygen ions is put on the positive x axis. The same operations for 455 313 other combinations of oxygen ions were also carried out and all of them were placed on the same xy plane. Figure 7a is the plot of oxygen ions in Z64 as dots on the xy plane. Some oxygen ions neighboring the three oxygen ions within the z-direction distance from the xy plane of ±0.5 Å are also plotted. The oxygen ion plot on the x axis is a straight line because the distance between the origin and the oxygen ion is varied. The other two oxygen ions are placed at the second quadrant and the third quadrant with a certain value of expanse, respectively. Those positions are labeled as A, B, and C. In Figure 7a, it is clearly seen that

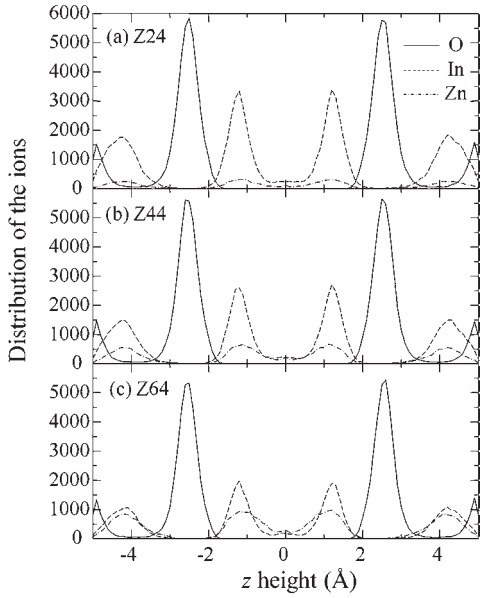

Figure 8. Ion distribution along the *z*-axis, which existed within 1 Å from *xy* plane origin for Z24, Z44, and Z64. Solid lines, dotted lines, and dashed-dotted lines represent O, In, and Zn, respectively.

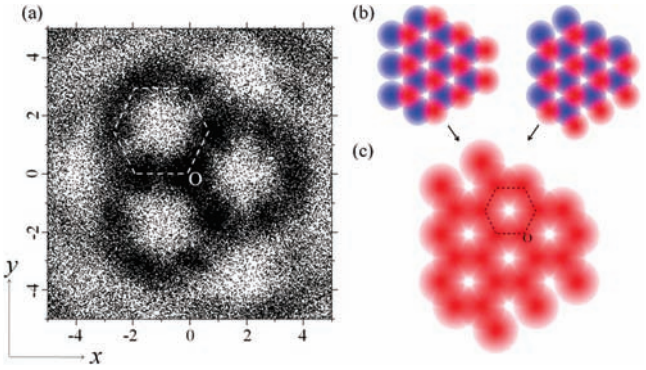

Figure 9. (a) Distribution of oxygen ions of Z64 with height from 2.25 to 2.75 Å on *xy* plane with *xy* range of 10 × 10 Å. Dot represents an oxygen ion. (b) Illustrations of two types of oxygen stacking at second layer above closed-packed structure of first layer. (c) Overlapped picture of two types of oxygen stacking layer.

there are some positions in which the density of oxygen ion dots is relatively high except at A, B, and C. These are labeled from D to L, indicating the high probability of oxygen ion existence. It is clearly shown that BCDEFG, CAGHIJ, and ABJKLD form a hexagonal shape, suggesting the existence of the quasi close-packed structure of oxygen ions. Accordingly, any 12 oxygen ions make a close packed structure on a plane as illustrated in Figure 7b. Next, let us see the *z* axis direction. Figure 8 shows the distribution of the ions along the *z*-axis, which existed within 1 Å from the origin of the *xy* plane for Z24, Z44, and Z64. The In and Zn ions located at a height of about ±1.2 Å from the *xy*-plane, while oxygen ions were at a height of about ±2.5 Å. This also confirmed the local layer structure in the a-IZO thin films. The distribution of the oxygen ions with the height from 2.25 to 2.75 Å of Z64 is shown in Figure 9a. We can see hexagonally arranged positions having high dot concentration. This arrangement can be explained as follows: When oxygen ions form an almost close-packed structure on the *xy* plane at $z = 0$, there are two types of stacking oxygen ions above the first layer. Three of six possible positions are occupied by the second layer oxygen ions at a height of about 2.5 Å (Figure 9b). In our reduced atomic arrangement, these two types cannot be distinguished because they are placed on the same *xy* plane. Therefore, in the oxygen ion dot map, we only see the overlapped picture of these two types of configuration (Figure 9c), which causes a hexagonal arrangement of positions having high dot concentration.

Using the reduced atomic arrangement, we can discuss the oxygen coordination number of In and Zn ions. Both In and Zn ions are at the plane with the height of about 1.25 Å above the *xy* plane, as seen in Figure 8. This height value agrees with that in the case of an octahedral site of the close-packed structure in which a cation is coordinated by three oxygen ions on the *xy* plane and three oxygen ions located on the plane at a height of 2.5 Å. In Figure 8, In ion distribution does not change, meaning that almost all of the In ions are located at the octahedral site for Z24, Z44, and Z64. On the other hand, the Zn ion distribution curve shows a peak growing at the lower positions with increasing ZnO content. The tetrahedral site in the close-packed structure of oxygen is coordinated by three oxygen ions on the *xy*-plane and one oxygen ion at height of 2.5 Å. The position of the cation is 0.6 Å above the *xy*-plane, which is lower than that of the cation in the octahedral site. Accordingly, the peak growing at the lower position means that a certain number of Zn ions occupy the tetrahedral site and the number depends on the ZnO content. When a Zn ion is in a tetrahedral site, In ions can hardly occupy the nearest-neighbor octahedral site due to the cation charge repulsion. This indicates that the area around the tetrahedral site occupied by a Zn ion is disarranged, preventing In ions from being ordered as in the bixbyite In_2O_3 crystal. As a result, it is suggested that the increase of ZnO content improves the stability of the amorphous phase in the a-IZO thin films by obstructing the regular arrangement of octahedral In ions.

5. Conclusion

The structures of a-IZO thin films were investigated using a combination of X-ray diffraction measurements and MD simulations. The characteristic amorphous structure having high oxygen coordination number and edge-shared polyhedra was confirmed both experimentally and through calculation. It was found that the structural properties such as coordination numbers and linkage patterns of polyhedra depended on the ZnO content in a-IZO thin films. FSDP in the interference functions revealed that there was a layer-like structure in the films. The reduced atomic arrangement for the structural model was introduced, and it demonstrated that the oxygen close-packed structure was realized in the nanometer range. From the discussion of site selective occupancy of In and Zn ions in the oxygen closed-packed structure, we conclude that the enhancement of the amorphous structure stability of a-IZO thin films could be explained by the effect of Zn ions obstructing In ions ordering in the octahedral site. These results that were reached using the reduced atomic arrangement provided considerable insight into the structure of the a-IZO thin films at an atomic level.

Acknowledgment. The authors thank Dr. K. Inoue of Idemitsu Kosan Co., Ltd. for providing the high quality IZO ceramic targets.